Object-oriented modelling and simulation for the ALFRED dynamics

Roberto Ponciroli, Andrea Bigoni, Antonio Cammi, Stefano Lorenzi, Lelio Luzzi*

Politecnico di Milano, Department of Energy, CeSNEF (Enrico Fermi Center for Nuclear Studies), via Ponzio 34/3, 20133 Milano, Italy

Article history:
Received 18 April 2013
Received in revised form
12 October 2013
Accepted 18 October 2013

1. Introduction

The Lead-cooled Fast Reactor (LFR) has been selected by the Generation IV International Forum as one of the candidates for the next generation of Nuclear Power Plants (NPPs) (GIF, 2002). Advanced reactor concepts cooled by Heavy Liquid Metal (HLM) coolants ensure a great potential for plant simplifications and higher operating efficiencies compared to other coolants, introducing however additional safety concerns and design challenges, and thus necessitating verifiable computational tools for transient design-basis analyses. This capability would enable designers to compare operational and safety aspects of design alternatives in order to finalize a model-based control strategy, supported by the results of dedicated plant simulators. The plant simulator should allow to verify the effectiveness of the proposed control scheme. Only after this preliminary stage, once the system governing dynamics has been characterized, it is possible to investigate potential control strategies and the way of coordinating the several operational modes. In particular, for LFR plants, the need of developing a proper control system has been recognized due to the technological issues brought by the use of lead as coolant (Tucek et al., 2006).

In this paper, the development of a simulation tool for studying the plant control-oriented dynamics of the Advanced Lead-cooled Fast Reactor European Demonstrator (ALFRED) is presented. ALFRED is a pool-type, small power reactor (Alemberti et al., 2010) conceived to be fully representative of the industrial scale reference system, and thus it is provided with a Balance of Plant (BoP) and envisaged to be connected to the electrical grid. Accordingly, a very flexible, straightforward and fast-running (i.e., without significant computational burden and implementation-related efforts) dynamics simulator has been sought, expressly meant for this early phase of the control system design, in which all the system specifications are still considered open design parameters and thus may be subject to frequent modifications. Such a tool has been specifically conceived to simulate the reactor response to typical transient initiators with the main purpose of laying the foundations for establishing viable control strategies. In a control-oriented perspective, the most important features (Cammi et al., 2005;

* Corresponding author.
E-mail address: lelio.luzzi@polimi.it (L. Luzzi).

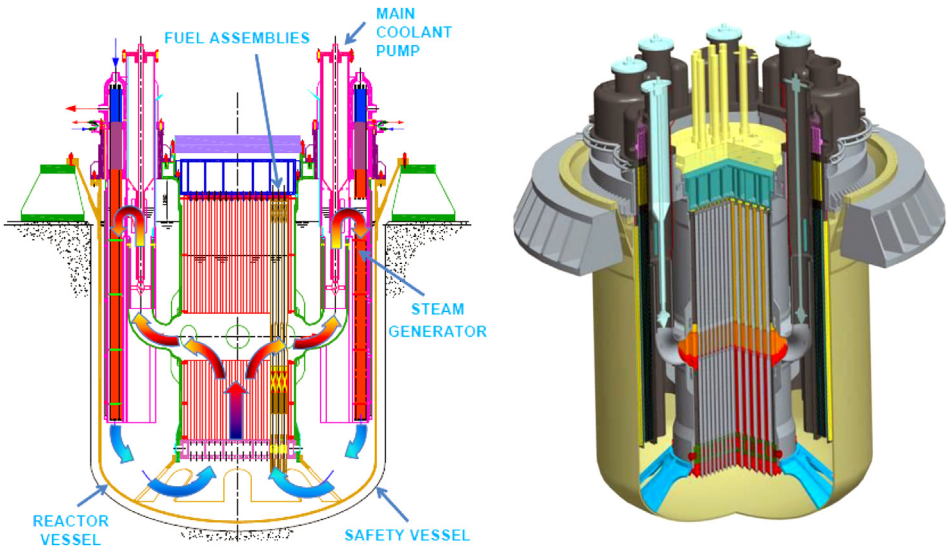

Fig. 1. ALFRED nuclear power plant layout (Alemberti et al., 2013).

Cammi and Luzzi, 2008) required to the modelling tool are the following: (i) *modularity*, in order to enhance the reusability of pre-existing and also validated components; (ii) *openness*, since the equations implemented have to be clearly readable; (iii) *efficiency*, meaning that the simulation code should be fast running; and (iv) *integrability* with the control system model.

A viable path to achieve the above-mentioned goals is constituted by the adoption of the Modelica language (Modelica, 2011). Introduced in 1997, Modelica is "a language for modelling and simulation of complex cyber-physical systems" (Fritzson, 2004). In particular, it is an object-oriented modelling approach specifically designed for the study of engineering system dynamics. In this perspective, Modelica facilitates the system description in terms of physical and engineering principles (i.e., mass, energy and momentum balance equations). Modelica is employed for the modelling of general physical phenomena described by sets of differential algebraic and discrete equations, supporting a declarative language. This feature allows *acausal modelling*, i.e., the direct use of equations without imposing the classic input/output declaration, granting a more flexible and efficient data flow (Fritzson, 2011). Finally, Modelica is open-source and it has already been successfully adopted in different fields, such as automotive, robotics, thermo-hydraulic and mechatronic systems, but also in nuclear simulation field (Cammi et al., 2005; Souyri et al., 2006).

As a consequence of the above mentioned considerations, a dynamic simulator of the ALFRED reactor has been realized by adopting the Modelica object-oriented language. The primary and secondary systems have been modelled and implemented in Modelica by assembling conventional component models already available in a specific thermal-hydraulic library, named *Thermopower* (Casella and Leva, 2006), and specifically developed nuclear component models, taken from the *NuKomp* library (Cammi et al., 2005), modified in order to provide the required capabilities for the analysis. The resulting overall plant simulator, incorporating also the BoP, consists of the following essential parts: core, steam generator, primary and secondary pumps, cold and hot legs, cold pool, turbine, and condenser. Finally, design-basis transient scenarios have been simulated and discussed to analyse the overall system free dynamics. The main purpose of this work is the realization of a preliminary "engineering simulator" to predict the reactor responses to typical transient initiators, involving not only the primary side, but also considering the secondary one and, in the future, the electrical grid connection.

The paper is organized as follows. In Section 2, a brief introduction to the ALFRED reactor is provided and its main features are reported. In Section 3, the adopted modelling approach is presented and the components used in the developed object-oriented simulator of the overall plant are described. Finally, some operational transients have been simulated and the obtained results are discussed (Section 4).

2. Reference reactor description

ALFRED is a small-size (300 MW_{th}) pool-type LFR. Its primary system current configuration (Alemberti et al., 2013) is depicted in Fig. 1. All the major reactor primary system components, including core, primary pumps, and Steam Generators (SGs), are contained within the reactor vessel, being located in a large lead pool inside the reactor tank. The coolant flow coming from the cold pool enters the core and, once passed through the latter, is collected in a volume (hot collector) to be distributed to eight parallel pipes and delivered to as many steam generators. After leaving the SGs, the coolant enters the cold pool through the cold leg and returns to the core.

The ALFRED core is composed by wrapped hexagonal Fuel Assemblies (FAs) with pins arranged in a triangular lattice (Fig. 2). The 171 FAs are subdivided into two radial zones with different plutonium enrichment guaranteeing an effective power flattening, and surrounded by two rows of dummy elements (geometrically identical to the fuel assemblies but not producing thermal power) serving as reflector. Two different and independent control rods systems have been foreseen, namely, Control Rods (CRs) and Safety Rods (SRs). Power regulation and reactivity swing compensation during the cycle are performed by the former, while the simultaneous use of both is foreseen for scram purposes, assuring the required reliability for a safe shutdown (Grasso et al., 2013). In Table 1, the major preliminary nominal parameters employed are presented.

Each of the eight SGs incorporated in ALFRED (Fig. 3) consists of a bundle of vertical bayonet tubes. The latter are constituted by an external safety tube and an internal insulating layer (delimited by a slave tube), which is aimed at ensuring the production of superheated dry steam since the high temperature difference between the rising steam and the descending feedwater may promote steam condensation in the upper part of the SG without a proper insulation. The gap between the outermost and the outer bayonet tube

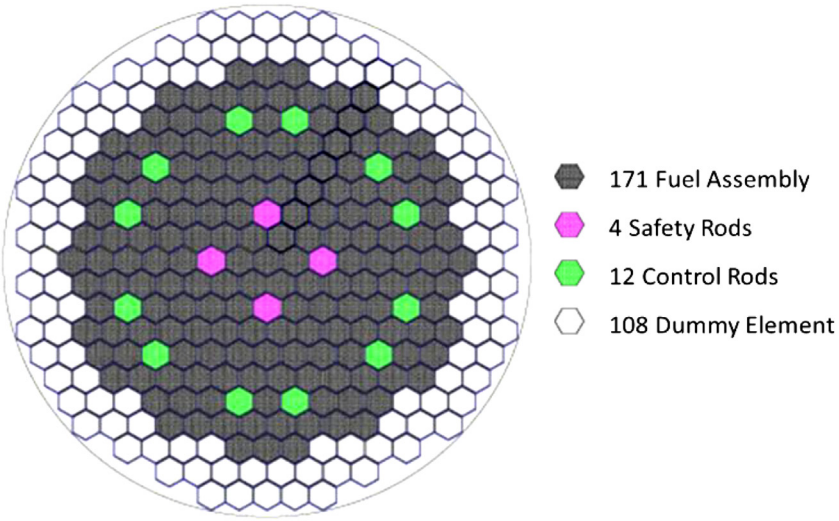

Fig. 2. ALFRED core configuration (Alemberti et al., 2013).

provides mechanical decoupling between the components, and is filled with pressurized helium and high thermal conductivity particles to enhance the heat exchange capability (Alemberti et al., 2013; Damiani et al., 2013). The feedwater from dedicated headers flows in the slave tube and, after reversing the motion at the bottom, rises along the annulus between inner and outer tubes. On the primary side, lead flows downwards axially along the outermost tube. In Table 2, the main SG parameters and specifications are listed.

3. Simulator development

A non-linear one-dimensional model of the ALFRED reactor has been developed by adopting the object-oriented approach based on the Modelica language. The overall system model has been built by connecting the different components (*objects*) through rigorously defined interfaces (*connectors*) corresponding to specific physical interactions occurring with the external environment or other objects. One of the main advantages of employing the Modelica language is the possibility of adopting *acausal modelling* approach. The system dynamics is described in terms of conservation laws that, combined with the constitutive equations of the components, determine the overall set of equations to be solved. Thanks to the acausal modelling, the equations of each component model can be written independently from the definitions of input/output variables. Thus, the causality of equation-based models is unspecified and becomes fixed only when the corresponding equation systems have to be solved (Fritzson, 2004). In this way, models are much easier to write and reuse, while the burden of determining the actual sequence of computations required for the simulation is entirely left to the compiler. In the common practice, most of the present simulators are based on causal modelling (MATLAB® and SIMULINK® software, 2005), whose main features are reported in Table 3.

Table 1
ALFRED preliminary core parameters (Grasso et al., 2013; Sciora, 2013).

Parameter	Value		Unit
Core			
Thermal power	300		MW_{th}
Coolant mass flow rate, Γ	25984		kg s^{-1}
Total number of FAs	171		–
Pins per FA	127		–
Coolant inlet temperature, T_{in}	400		°C
Coolant outlet temperature, T_{out}	480		°C
Fuel pin			
Cladding material	15-15-Ti		–
Fuel material	MOX		–
Cladding outer radius	$5.25 \cdot 10^{-3}$		m
Cladding inner radius	$4.65 \cdot 10^{-3}$		m
Pellet outer radius	$4.50 \cdot 10^{-3}$		m
Pellet inner radius	$1.00 \cdot 10^{-3}$		m
Active height	0.6		m
Reactivity and kinetic coefficients	*BoC*	*EoC*	
Doppler constant, K_D	−555	−566	pcm
Lead expansion coefficient, α_L	−0.271	−0.268	pcm K^{-1}
Axial clad expansion, α_{CZ}	0.037	0.039	pcm K^{-1}
Axial wrapper tube expansion, α_{WZ}	0.022	0.023	pcm K^{-1}
Radial clad expansion, α_{CR}	0.008	0.011	pcm K^{-1}
Radial wrapper tube expansion, α_{WR}	0.002	0.003	pcm K^{-1}
Axial fuel expansion (linked case), α_{FZ}	−0,232	−0,242	pcm K^{-1}
Diagrid expansion, α_{Dia}	−0,147	−0,152	pcm K^{-1}
Pad expansion, α_{Pad}	−0,415	−0,430	pcm K^{-1}
Reactor lifetime, Λ	$6.116 \cdot 10^{-7}$	$6.296 \cdot 10^{-7}$	s
Delayed neutron fraction, β	336	335	pcm

In addition, the multi-physics approach of the Modelica language must be mentioned. General in scope, it provides modelling primitives such as generic algebraic, differential and difference equations, and it is not tied to any specific physical or engineering domain (i.e., mechanics, electrical engineering, or thermodynamics). Thus, it is quite straightforward to describe multi-disciplinary systems, such as the reactor core, where several physics (e.g., neutronics, heat exchange and fluid dynamics) interact with each other. Furthermore, a more realistic plant representation is made possible by the component-based description. As simulation environment, Dymola (Dynamic Modelling Laboratory) (Elmqvist et al., 1993) has been adopted, as dedicated libraries of validated models for power plant components are available.

As to the efficiency of the simulation code, Modelica compilers incorporate sophisticated symbolic manipulation algorithms, which allow to obtain index-1 systems of differential-algebraic equations from higher-index ones, to symbolically solve both linear and nonlinear model equations (Fritzson, 2004). The resulting code is then linked to state-of-the-art numerical integration codes such as DASSL (Brenan et al., 1989). As shown in Fig. 4, the ALFRED object-oriented model has been built by connecting the plant single components. In the following sub-sections, the components specifically modelled in this paper (i.e., core, steam generator, turbine) will be

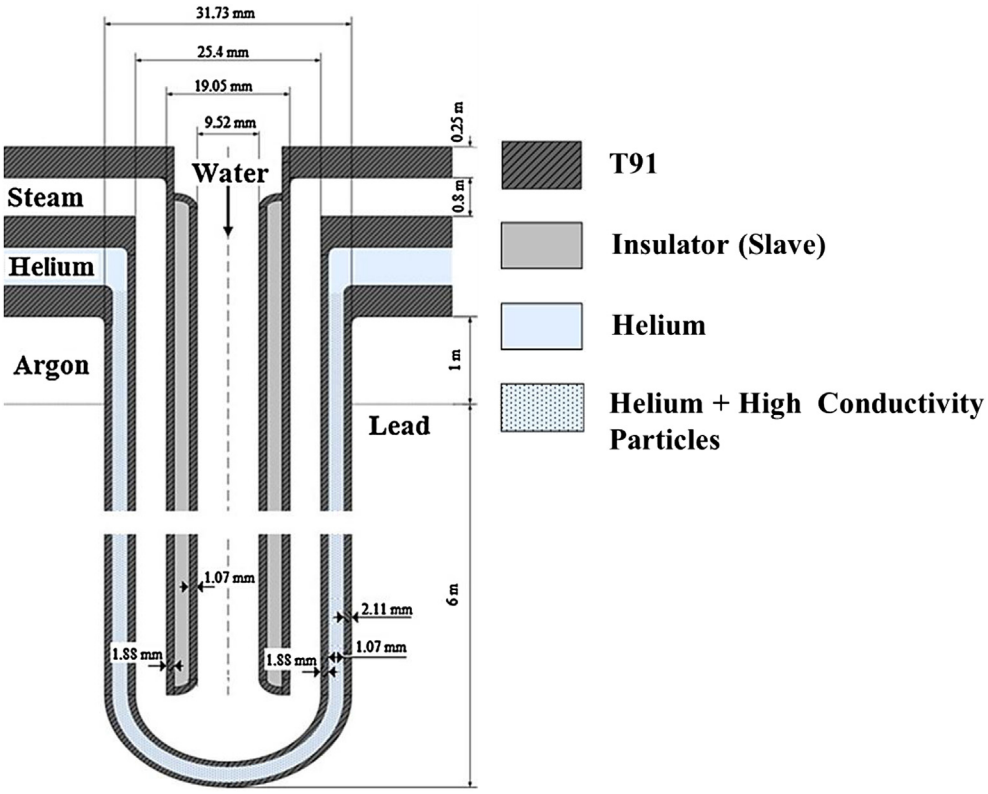

Fig. 3. ALFRED bayonet tube SG configuration (not in scale) (Alemberti et al., 2013; Damiani et al., 2013).

described in some detail, whereas for the most conventional ones we mainly refer to (Casella and Leva, 2006).

3.1. Core

As far as the ALFRED core is concerned (Fig. 5), point reactor kinetics and one-dimensional heat transfer models have been implemented, coherently with the plant specifications, by incorporating suitable geometry, material properties and correlations, neutronic feedback coefficients and kinetic parameters (Table 1).

The component-based core model is constituted by four subsystems, each one dedicated to a particular physics. The component *Kinetics* implements a point reactor kinetics model with one neutron energy group and eight Delayed Neutron Precursor (DNP) groups. Therefore, the neutron density evolution is described by the following equation:

$$\frac{dn}{dt} = \frac{\rho - \beta}{\Lambda} n + \sum_{i=1}^{8} \lambda_i c_i + q \tag{1}$$

the corresponding concentration of precursors being expressed as

$$\frac{dc_i}{dt} = \frac{\beta_i}{\Lambda} n - \lambda_i c_i \quad i = 1{-}8 \tag{2}$$

In the present model, two different definitions have been implemented to describe the effective fuel temperatures, and namely: T_f^D, which expresses the effective temperature to allow for the Doppler effect, and T_f^{eff}, which represents the average temperature that

Table 2
ALFRED SG major nominal parameters (Alemberti et al., 2013; Damiani et al., 2013).

Parameter	Value		Unit
Single SG parameter			
Power	37.5		MW
Feedwater inlet temperature	335		°C
Steam outlet temperature	450		°C
Steam pressure	180		bar
Length of heat exchange	6		m
Number of tubes	510		–
	Outer diameter	*Thickness*	
Slave tube	$9.52 \cdot 10^{-3}$	$1.07 \cdot 10^{-3}$	m
Inner tube	$19.05 \cdot 10^{-3}$	$1.88 \cdot 10^{-3}$	m
Outer tube	$25.40 \cdot 10^{-3}$	$1.88 \cdot 10^{-3}$	m
Outermost tube	$31.73 \cdot 10^{-3}$	$2.11 \cdot 10^{-3}$	m

Table 3
Main features and differences between causal and acausal approach.

Causal approach	Acausal approach
System input and output variables have to be established at the beginning	It is not necessary to establish *a priori* input and output variables
Equations have to be rewritten for each specific application in state space representation	Causality remains unspecified as long as equations have to be solved
Low flexibility in changing the model configuration	More realistic description of components and modularity
Low reusability of previous work. According to the applicative context, problem formulation as a series of operations has to be carried out by the user	Possibility of easily reusing previously developed models. Components models are defined independent of their potential connections (*inheritance*)
Block diagram representation (physics-oriented)	Plant representation (component-oriented)
Integration algorithm for ordinary differential equations (lower computational cost)	Integration algorithm for differential algebraic equations (higher computational cost)
Low order modelling, easy to linearize	Potentially high number of equations involved

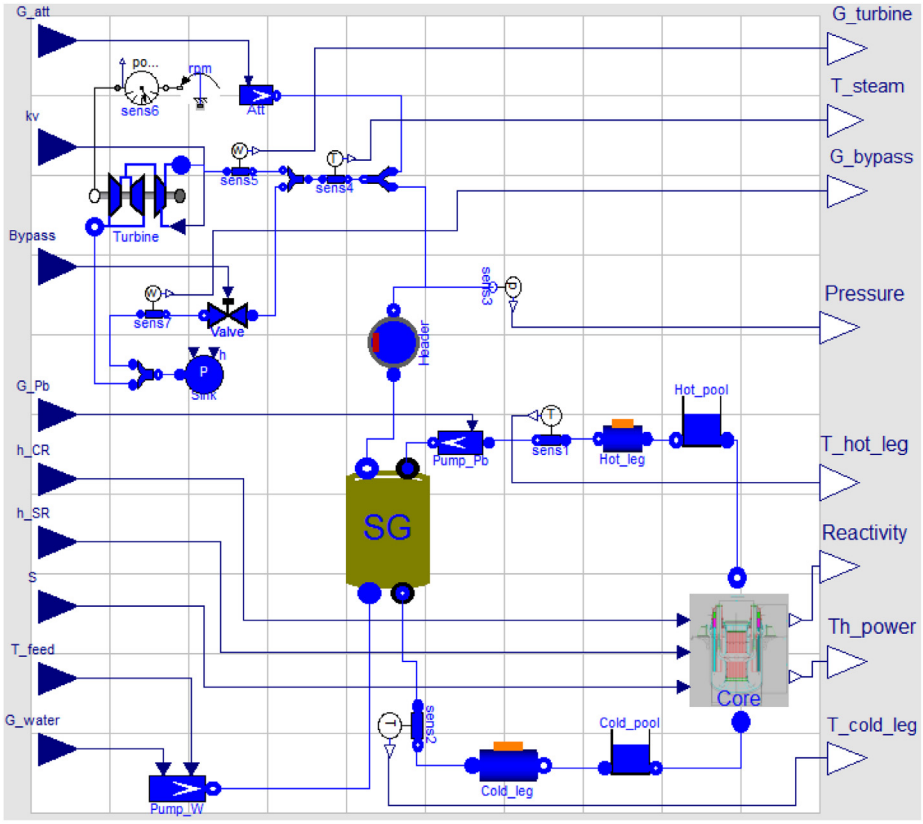

Component	Description
Core	Reactor core
Cold_pool	Pool collecting the lead coming from the SG outlet
Cold_leg	Collector between the SG outlet and the core inlet
Hot_pool	Pool collecting the lead coming from the core outlet
Hot_leg	Collector between the core outlet and the SG inlet
sens	Temperature and pressure sensor placed in the plant
Pump_Pb	Lead axial pump
SG	Steam generator
Header	Volume collecting the produced steam
Pump_W	Water pump
Turbine	Steam turbine unit
Sink	Condenser
Att	Attemperator allowing to regulate the steam temperature

Input variable	Definition
G_att	Attemperator mass flow rate
kv	Turbine admission valve coefficient
Bypass	Bypass valve coefficient
G_Pb	Primary circuit lead mass flow rate
h_CR	Control rod height
h_SR	Safety rod height
S	Neutron source
T_feed	Feedwater inlet temperature
G_water	Feedwater mass flow rate

Output variable	Definition
G_turbine	Turbine admitted mass flow rate
T_steam	Turbine inlet steam temperature
G_bypass	Bypass discharged mass flow rate
Pressure	SG pressure
T_hot_leg	Temperature of lead flowing out of the core
Reactivity	System reactivity
Th_power	Thermal power produced within the core
T_cold_leg	Temperature of lead flowing into the core

Fig. 4. ALFRED object-oriented model. In the legend, the defined input and output variables are reported in order to allow the comprehension of the graphical interface.

allows to evaluate quantitatively the reactivity feedback due to the pellet deformation caused by thermal stresses. Therefore, as far as the Doppler reactivity contribution is concerned, an effective fuel temperature allowing for resonances broadening (Kozlowski and Downar, 2006) has been considered:

$$T_f^D = 0.3 \cdot T_f^1 + 0.7 \cdot T_f^3 \tag{3}$$

In Eq. (3), T_f^1 and T_f^3 represent the average temperatures in the central region and in the external one of the fuel pin, respectively (see Fig. 6). In Eq. (4), the weights provide an estimate of the volume-weighted average behaviour, and have been used to reproduce the parabolic trend of the temperature field within the fuel pellets:

$$T_f^{eff} = (1/2) \cdot T_f^1 + (1/2) \cdot T_f^3 \tag{4}$$

The reactivity variation from a generic fuel temperature distribution T_{f1} (with effective average T_{f1}^D) to a fuel temperature distribution T_{f2} (with effective average T_{f2}^D), due to the Doppler effect, has been evaluated as follows (Waltar et al., 2012):

$$\Delta\rho\left[T_{f1} \rightarrow T_{f2}\right] \approx 1.1 \cdot K_D \left(\ln \frac{T_{f2}^D}{T_{f1}^D}\right) \tag{5}$$

Reactivity effects due to the coolant density variations, as well as to the axial and radial expansions, have been taken into account by adopting linear equations with constant coefficients. In particular, axial and radial cladding expansions have been related to the average cladding thermal conditions, while axial and radial wrapper expansions have been considered governed by the lead temperature. On the other hand, the grid expansion effect concerns the increase of the core radius due to the incoming coolant temperature enhancement. Therefore, the coolant volume inside core increases as well as the core volume and, in turn, the leakages. These combined effects determine an overall negative contribution. The pad effect is determined by the radial expansion difference between the bottom of the subassemblies at the incoming coolant temperature and their top at the outlet coolant temperature.

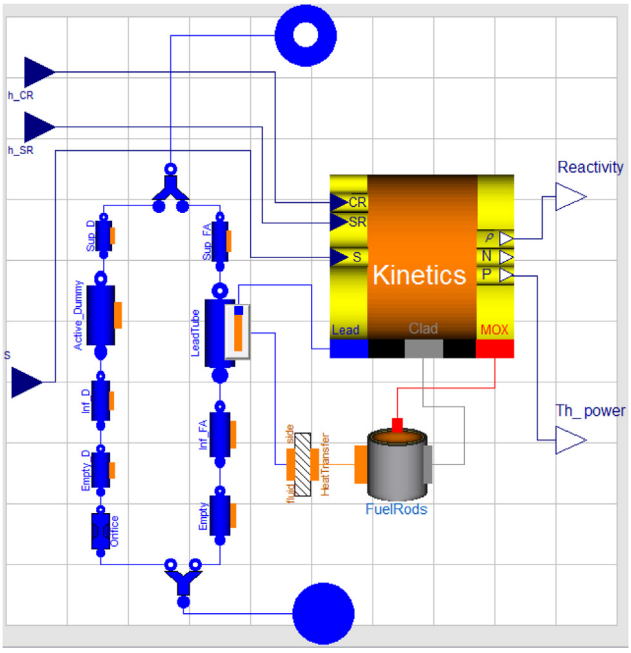

Fig. 5. ALFRED core object-oriented model.

However, this reactivity contribution is quite reduced (Sciora, 2013).

As far as the CRs are concerned, a reactivity differential curve has been adopted based on the reactivity worth of the 12 rods at different insertion lengths (Fig. 7). On the other hand, worth characterization of SRs does not require such an accuracy, because these rods are extracted during start-up phase and then they are kept out of the core while the reactor is operating at full power conditions. Consequently, a linear dependence of the reactivity as function of axial position is sufficient to describe the SR reactivity contribution.

The overall system reactivity is given by the sum of the various contributes, as follows:

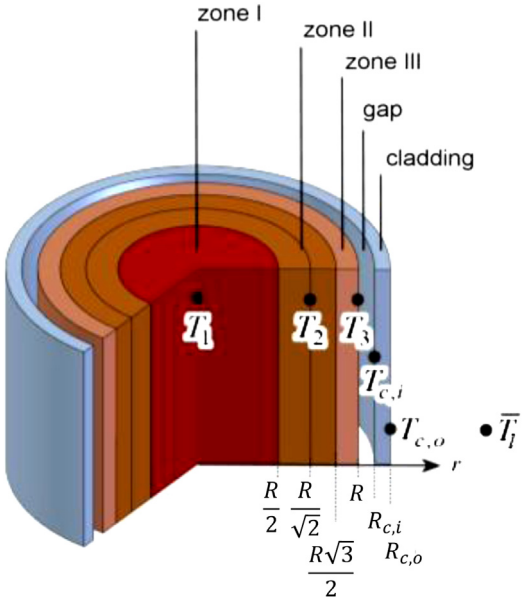

Fig. 6. Fuel pin radial scheme for heat transfer modelling.

$$\rho(t) = \rho_0 + \alpha_L \cdot (T_l - T_{l,0}) + 1.1 \cdot K_D \left(\ln \frac{T_{f2}^D}{T_{f1}^D} \right) + \alpha_{CZ} \cdot (T_c - T_{c,0}) + \alpha_{WZ} \cdot (T_l - T_{l,0}) + \alpha_{CR} \cdot (T_c - T_{c,0}) + \alpha_{WR} \cdot (T_l - T_{l,0}) + \alpha_{FZ} \cdot (T_c - T_{c,0}) + \alpha_{Dia} \cdot (T_{l,in} - T_{l,in,0}) + \alpha_{Pad} \cdot (T_{l,out} - T_{l,out,0}) + A_{CR} \cdot \sin(B_{CR} \cdot h_{CR} + C_{CR}) + D_{CR} + A_{SR} \cdot \frac{(h_{SR} - x_{SR})}{L_{SR}} \quad (6)$$

The terms in Eq. (6) represent the initial reactivity margin, the effect due to lead density, Doppler effect, axial cladding expansion, axial wrapper expansion, radial cladding expansion, radial wrapper expansion, axial fuel expansion, diagrid expansion, pad effect, control rod contribution, and safety rod contribution, respectively.

The component *FuelRods* describes the thermal behaviour of the fuel pins, by adopting five radial regions within the element (i.e., cladding, gaseous gap and three concentric zones of equal volume within the pellet). The time-dependent Fourier equation is applied considering only the radial heat transfer, thus disregarding both the axial and the circumferential thermal diffusion. Fourier equation has been discretized radially in five zones and longitudinally in a user-defined number (N) of nodes.

$$d_f c_f \frac{\partial T_f}{\partial t} = \frac{1}{r} \frac{\partial}{\partial r} \left(r k_f \frac{\partial T_f}{\partial r} \right) + q''' \quad (7)$$

$$\frac{\partial}{\partial r} \left(r k_g \frac{\partial T_g}{\partial r} \right) = 0 \quad (8)$$

$$d_c c_c \frac{\partial T_c}{\partial t} = \frac{1}{r} \frac{\partial}{\partial r} \left(r k_c \frac{\partial T_c}{\partial r} \right) \quad (9)$$

The component *LeadTube* models the coolant flowing through the core channels represented as cylindrical conduits. It simulates a one-dimensional single-phase fluid flow with heat transfer from the fuel pin boundary and with temperature-dependent physical properties (OECD-NEA, 2007). This approach is based on distributed-parameter mass, momentum and energy conservation equations discretized by employing a finite volume method.

$$A \frac{\partial d}{\partial t} + \frac{\partial w}{\partial x} = 0 \quad (10)$$

$$\frac{\partial w}{\partial t} + A \frac{\partial p}{\partial x} + dgA \frac{\partial z}{\partial x} + \frac{C_f \omega}{2dA^2} w|w| = 0 \quad (11)$$

$$dA \frac{\partial h}{\partial t} + dAu \frac{\partial h}{\partial x} - A \frac{\partial p}{\partial t} = \omega \phi \quad (12)$$

Equations (10) and (11) describe the pressure and mass flow rate dynamics, while Eq. (12) describes the slower dynamics of heat transport with the fluid velocity.

The component *HeatTransfer* allows to evaluate the heat flux exchanged between two one-dimensional interacting objects (e.g., the fluid flow and metal wall) as a function of the corresponding surface temperatures. Since the fuel pins are arranged in a triangular lattice, the Ibragimov–Subbotin–Ushakov correlation (Cheng and Tak, 2006), Eq. (13), has been adopted to properly estimate the convective heat transfer coefficient. Moreover, among the possible correlations, it is the most conservative one since gives the lowest value of the Nusselt number.

$$Nu = 4.5 + 0.014 \cdot Pe^{0.8} \quad (13)$$

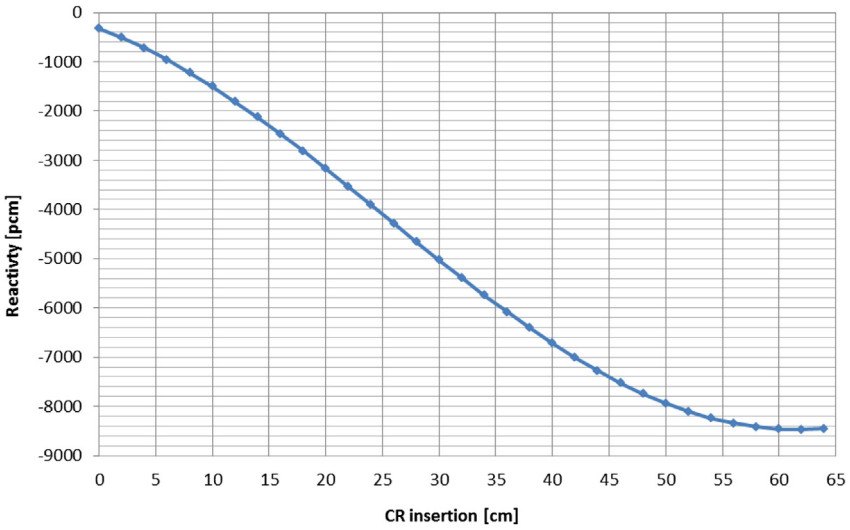

Fig. 7. Calibration curve of control rods and safety rods.

In the ALFRED core, the presence of a *bypass mass flow rate* has been foreseen since it has a fundamental role in certain plant operational modes, such as the start-up phase. In the proposed configuration, the main part of the coolant passes through the fuel elements, while a reduced fraction passes through the interstices between the wrappers, and through the dummy elements and the cases of the CRs and the SRs. Indeed, the power is deposited not only in the fuel, but also in the other materials, mainly due to the γ emission. For these reasons, the lead mass flow rate devoted to the bypass has been fixed at the 3% of the one that circulates in the primary circuit. In a preliminary description, in order to represent the evolution of the temperature fields of the main components of the core, the presence of the bypass mass flow rate can be neglected. This approach can be suitable if the system is studied only in nominal operating conditions. Nevertheless, in accidental scenarios or in operating conditions in which the lead mass flow rate is not kept constant at the nominal value, a more accurate characterization of the pressure field is essential. In particular, in the core thermal-hydraulics description, two types of channels, which represent the fuel elements and the dummy elements, have been allowed for.

In the modelling of the channels, in order to reproduce the actual layout of the assemblies (Fig. 8), different types of components (Fig. 9) have been employed. Furthermore, a component that allows to impose additional pressure losses has been added to the dummy elements description. Since the channels are subjected to the same inlet and the outlet pressure field, hydraulic resistance at the entrance of dummy elements has been suitably tuned so as to achieve the desired pressure field.

As far as the distributed losses within the coolant channels are concerned, they have been preliminarily estimated adopting the Mc-Adams correlation (Todreas and Kazimi, 2012) for the Fanning friction factor. On the other hand, the modelling of the form losses has turned out to be difficult since the dimensional specifications concerning the spacers have not been assessed yet. At this point, since the total pressure losses are specified in the core design and the distributed ones have been evaluated, it has been easy to obtain the contribution of the form losses, representing the influence of the spacers in the core thermal-hydraulics by using the dedicated component *Orifice*, which allows to implement a suitable hydraulic resistance.

All the several core subsystems have been eventually connected. In particular, the mutual influences between neutronics and thermal-hydraulics have been taken into account by means of the above mentioned feedback reactivity coefficients represented in the Modelica language through dedicated *connectors*. As shown in

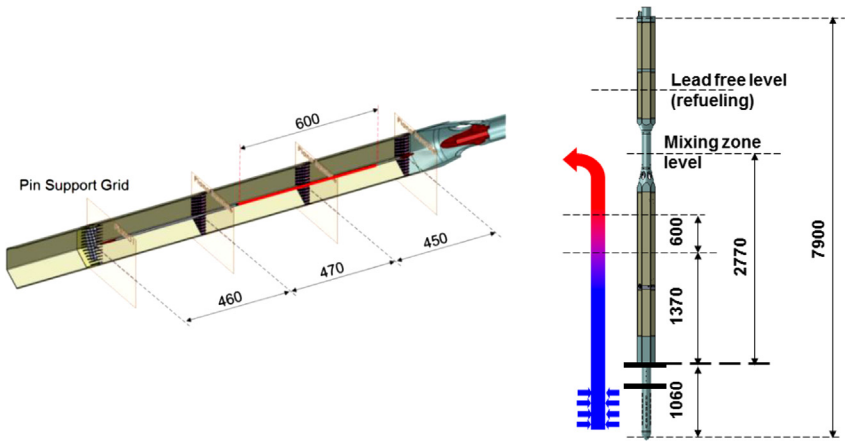

Fig. 8. Fuel assembly geometry (lengths are expressed in mm).

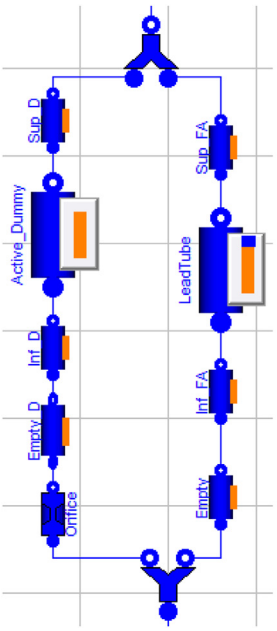

Component	Description
Sup D	Upper region of dummy elements
Active_Dummy	Region of dummy elements corresponding to the active zone of fuel assemblies
Inf D	Lower region of dummy elements
Empty D	Empty region of dummy elements
Orifice	Form pressure drop which allow to achieve the real pressure field
Sup FA	Upper region of fuel assemblies
LeadTube	Active region of fuel assemblies
Inf FA	Lower region of fuel assemblies
Empty	Empty region of fuel assemblies

Fig. 9. Detailed view of ALFRED core: representation of coolant channels.

Fig. 5, blue, grey and red (in web version) connectors allow to carry the information about lead, cladding and fuel thermal behaviour in order to consider their influence on the neutronics.

3.2. Hot and cold pool

The coolant hot and cold pool models (named *Hot_pool* and *Cold_pool*) have been implemented by employing a component describing a free-surface cylindrical lead tank (responsible for most of the large thermal inertia characterizing the overall system), on which mass and energy balances have been taken, assuming that no heat transfer occurs, except through the inlet and outlet boundaries.

3.3. Hot and cold legs

In order to represent transport phenomena, simple one-phase *LeadTube* components have been employed (named *Hot_leg* and *Cold_leg*). One-dimensional flow models have been implemented, neglecting thermal dispersion, to properly consider the time delays due to transport phenomena between the core and the SGs, and between the SGs and the cold pool.

3.4. Pumps

As far as the primary and secondary pumps are concerned, ideal flow rate regulators have been employed.

3.5. Steam generator

Due to its non-conventional bayonet-tube design, an effort has been spent to set up a specific component representing the ALFRED SG (Fig. 10). A simplified description has been adopted, based on a one-dimensional description of the actual geometry, which has been reproduced by means of different tube models connected together. In this way, the advantage of reusability of the Modelica models has been exploited. Indeed, the same tube, based on a certain set of equations, can be employed in different contexts and then extended through *inheritance* by adding further equations.

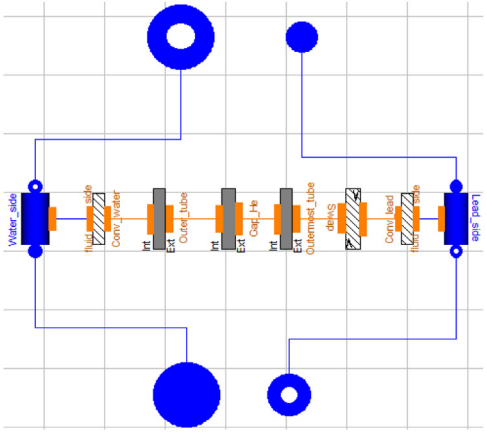

Component	Description
Water_side	Tube model that describes the water flowing
Conv_water	Component that describes the convective heat transfer on water side
Outer_tube, Gap_He, Outermost_tube	Components that allows for the conduction phenomena within the different interfaces
Swap	Component that allows to reproduce the counter-current configuration.
Conv_lead	Component that describes the convective heat transfer on lead side
Lead_side	Tube model that describes the lead flowing

Fig. 10. ALFRED SG object-oriented model.

After entering the SG, water flows down in the slave tube (Fig. 3) and there is no heat exchange neither thermal dispersion, thanks to the effective insulation provided. Thus, water conditions at the SG inlet and at the bottom of the tube are the same. For this reason, this first part has been neglected and the feedwater has been simulated to flow directly in a counter-current configuration, exchanging thermal power with the external lead. The component geometry has been substituted with concentric tube bundles in a counter-current flow configuration where the pressure drops are concentrated at the bayonet bottom (i.e., where the fluid flow reverses). A turbulent, lumped pressure drop model has been assumed, proportional to the kinetic pressure.

As far as the water side is concerned, a tube allowing to describe a two-phase fluid has been selected, adopting averaged densities in the neighbourhood of phase changes so as to avoid non-physical simulation artefacts due to phase change discontinuities at the model nodes. A two-phase homogeneous model (i.e., with the same velocity for the liquid and vapour phases) has been adopted. Water-side convective heat transfer coefficients have been evaluated by implementing the Dittus–Boelter correlation for one-phase regions, and the Kandlikar correlation for the boiling region (Todreas and Kazimi, 2012). According to the latter correlation, the two-phase heat transfer coefficient, h_{TP}, is equal to the larger of $h_{TP,NBD}$ and $h_{TP,CBD}$, i.e., the two-phase heat transfer coefficients in the nucleate boiling dominant and convective boiling dominant regions, respectively. These coefficients are given by the following equations:

$$h_{TP,NBD} = 0.6683\mathrm{Co}^{-0.2}(1-x_v)^{0.8}f(\mathrm{Fr}_{LO})h_{LO} + 1058.0\mathrm{Bo}^{0.7}(1-x_v)^{0.8}F_{Fl}h_{LO} \quad (14)$$

$$h_{TP,CBD} = 1.136\mathrm{Co}^{-0.9}(1-x_v)^{0.8}f(\mathrm{Fr}_{LO})h_{LO} + 667.2\mathrm{Bo}^{0.7}(1-x_v)^{0.8}F_{Fl}h_{LO} \quad (15)$$

where $\mathrm{Co} = (d_L/d_v)^{0.5}[(1-x_v)/x_v]^{0.8}$ and $\mathrm{Bo} = q''/(w \cdot i_{LG})$ are the convection and boiling numbers, respectively. F_{Fl} is the fluid–surface parameter that incorporates the effect of surface and fluid properties, and allows to take into account differences in nucleating characteristics. h_{LO} is the single-phase heat transfer coefficient with all flow as liquid. The function $f(\mathrm{Fr}_{LO})$ is a Froude number with all flow as liquid. This parameter addresses the stratified flow region.

On the lead side, the component describing the behaviour of a single-phase fluid, previously used for the core model, has been adopted. Convective heat transfer coefficients have been evaluated by implementing the Ibragimov–Subbotin–Ushakov correlation as well. The multiple wall interfaces have been modelled by adopting different conductive-exchange elements, in which thermal resistance is computed according to the formulation of Fourier equation in cylindrical coordinates, while the heat capacity is lumped in the middle of the tube thickness. Dedicated components have been implemented to represent each interface constitutive layer (i.e., insulating layer, outer tube, helium gap, outermost tube). Besides, the *HeatTransfer* component has been used to evaluate the convective heat exchange on both water and lead sides, a *Swap* component has been adopted to allow for the counter-current configuration. In this way, temperature and flux vectors on one side are swapped with respect to the ones on the other side. Furthermore, only one SG with a suitably rescaled number of tubes guaranteeing a thermal power of 300 MW_{th} (instead of the actual eight 37.5 MW_{th} SGs) has been considered.

3.6. Outlet header

The steam coming out from the SG is suitably collected in a *header*, i.e., a well-mixed chamber having no pressure drop and no energy exchange with the environment that allows to dampen any pressure transient, limiting the impact on the conditions of the steam that flows into the turbine.

3.7. Attemperator

An attemperator has been foreseen between the outlet header and turbine, i.e., a reduced water mass flow rate at saturation conditions that is added to the steam flow. In this way, it is possible to promptly limit the steam temperature at the turbine inlet keeping this variable of interest as close as possible to its nominal value (450 °C).

3.8. Turbine unit

Particular attention has been paid to this component, which is fundamental to properly take into account the electrical power provided to the grid, and constitutes a crucial parameter in a control perspective. The component selected for the turbine model describes a simplified steam turbine unit in which a fraction of the available enthalpy drop is disposed by the High Pressure (HP) stage, whereas the remaining part by the Low Pressure (LP) one, with different time constants. A valve governs the overheated steam mass flow rate passing through the turbine. By adopting a simplified approach, choke flow conditions have been imposed. If the ratio of upstream pressure to downstream pressure is higher than the critical ratio ($x_c \approx 0.5$), in the section of maximum damping of the fluid vein a sonic shock wave is produced (Dolezal and Varcop, 1970). In this way, the inlet steam mass flow rate does not depend on the downstream pressure, namely:

$$\frac{p_{up}-p_{down}}{p_{up}} > x_c \quad \Rightarrow \quad w_v = A_v\lambda_c\sqrt{d_v(p)p} \quad (16)$$

Given that, it is possible to adopt the following approximation for the superheated steam:

$$d_v(p)p \propto p^2 \quad (17)$$

It follows that:

$$w_v \cong k_v p \quad (18)$$

Accordingly, the steam mass flow rate is regarded proportional to the inlet pressure and governed by operating the turbine admission valve (system input), not by throttling (i.e., no loss of thermodynamic efficiency occurs).

3.9. Bypass

After having passed through the SG, downstream of the temperature sensor, the steam mass flow rate can be subdivided into two ways (Fig. 11). The former is a pipe that leads to the turbine, whereas the latter constitutes a bypass that directly leads to the condenser. This “alternative way” performs a very important function in particular operative conditions of the secondary side, when the reactor is operating at very low power levels, such as during the start-up phase. Indeed, when the thermal power from the primary circuit is not sufficient to ensure the steam nominal conditions, the flow is directly disposed to the condenser to avoid jeopardizing the integrity of the turbine, which cannot process an incoming fluid in such conditions. On the other hand, when the

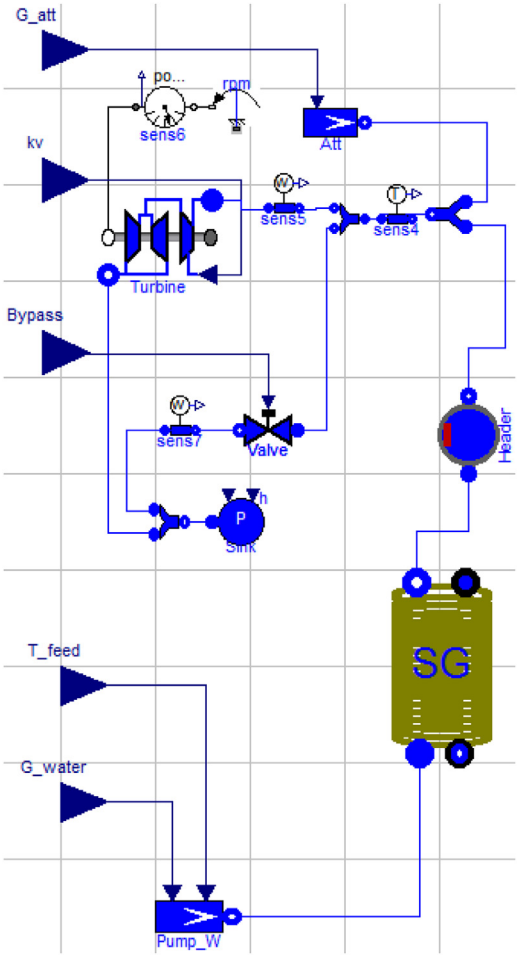

Fig. 11. ALFRED reactor secondary side.

power level allows to obtain overheated steam, it is possible to let it flow to the turbine, while the bypass way is progressively closed.

4. Simulations and results

The reactor response to typical transient initiators has been investigated. In particular, three scenarios have been simulated, i.e., feedwater mass flow rate reduction, turbine admission valve coefficient variation, and Unprotected Transient of OverPower (UTOP), starting from nominal full power steady-state operating conditions (Tables 1 and 2). The tool developed in the present work allows to simulate a transient of 2500 s requiring a computational time of less than 30 s (2.20 GHz with 8 GB memory), hence turning out to be suitable for control-oriented purposes.

4.1. Reduction of the feedwater mass flow rate

The dynamic response of the system to a 20% step reduction of the feedwater mass flow rate has been investigated. This transient is particularly relevant in a control perspective since the feedwater mass flow rate may be considered as one of the most promising control variables for the regulation of the cold pool lead temperature. In particular, the latter has to be kept as close as possible to its nominal value (400 °C). The main outcomes of this simulation scenario are the assessment of: (i) the dynamics of the transients, (ii) the influence of the feedwater mass flow rate on the lead temperature in the cold pool; (iii) the compliance of the other variables of interest with the operational or safety limits; (iv) the coupling between the primary and the secondary circuit. Indeed, the feedwater mass flow variation affects also the secondary circuit, the steam generation and the electrical power production. Moreover, in the common practice for nuclear reactor control, after an enhancement of the power request by the electrical grid, the feedwater mass flow rate is usually enhanced to fulfil the load demand. For these reasons, it is relevant to investigate the system dynamic behaviour both for the primary and the secondary side, following a feedwater mass flow rate variation.

For the first 70 s, the only component affected by the perturbation is the SG itself, while in the second part of the transient SG and core are strongly coupled in virtue of reciprocal feedbacks. Since the other operating conditions are not modified (the turbine admission valve is not operated), the first consequences are a nearly step-wise pressure reduction in the SG (Fig. 12a), a global worsening of the heat exchange conditions because of the combined effects of a reduced mass flow rate and a narrower temperature difference between primary and secondary fluids. Therefore, an increase of the lead SG outlet temperature occurs (Fig. 12b). When the hotter coolant begins to flow into the core, the lead average temperature increases (Fig. 12c), inducing an insertion of negative reactivity (Fig. 12d) that leads to a reduction of both core power and fuel temperature (Fig. 12e–f). Nevertheless, the coolant core outlet temperature (Fig. 12g) undergoes an increase, even if smaller than the inlet perturbation, and consequently hotter lead flows towards the SG inlet. The feedback to the secondary side is evident when examining the steam outlet temperature evolution (Fig. 12h). Indeed, it rises almost instantaneously after the perturbation, and, when the core power starts decreasing, it continues increasing but exhibiting a smaller and smaller gradient, consistently with the progressive thermal power reduction, to the final steady-state condition. From the free dynamics analysis, it is possible to assess the time constants characterizing this plant, which are key parameters for the development of the reactor control. In addition, relevant outcomes concerning the control action necessary to satisfy the operational constraints are highlighted. In particular, a strong control action has to be carried out in order to keep the SG pressure as close as possible to its nominal value (180 bar) avoiding depressurization. The same attention has to be paid to the steam temperature since hotter (or colder) vapour condition can jeopardize the turbine stages.

4.2. Variation of the turbine admission valve coefficient

In order to study the system behaviour after a change of the grid request, the system response after a 10% reduction of the turbine admission valve flow coefficient has been simulated. This is another fundamental transient for the control design since it allows evaluating the possibility of performing load-frequency regulation according to the grid demands by adopting this kind of reactor. In particular, in case of power decrease, the power regulation is achieved by closing the turbine admission valve. In this way, a lower steam mass flow rate circulates in the turbine and a lower mechanical power is available to the alternator. As far as the SGs are concerned, the pressure increase following the valve closing is compensated by a simultaneous control action performed both on feedwater mass flow rate and control rods in order to balance the power produced. This transient is relevant in the control strategy definition and characterization because of ALFRED is meant to be employed as a NPP connected to the electrical grid.

The first consequence of the performed perturbation is an instantaneous pressure rise within the SG (Fig. 13a) since in the simulated transient a coordinated control strategy is not carried out. Because of the secondary fluid sudden compression, the temperature difference between primary and secondary fluids

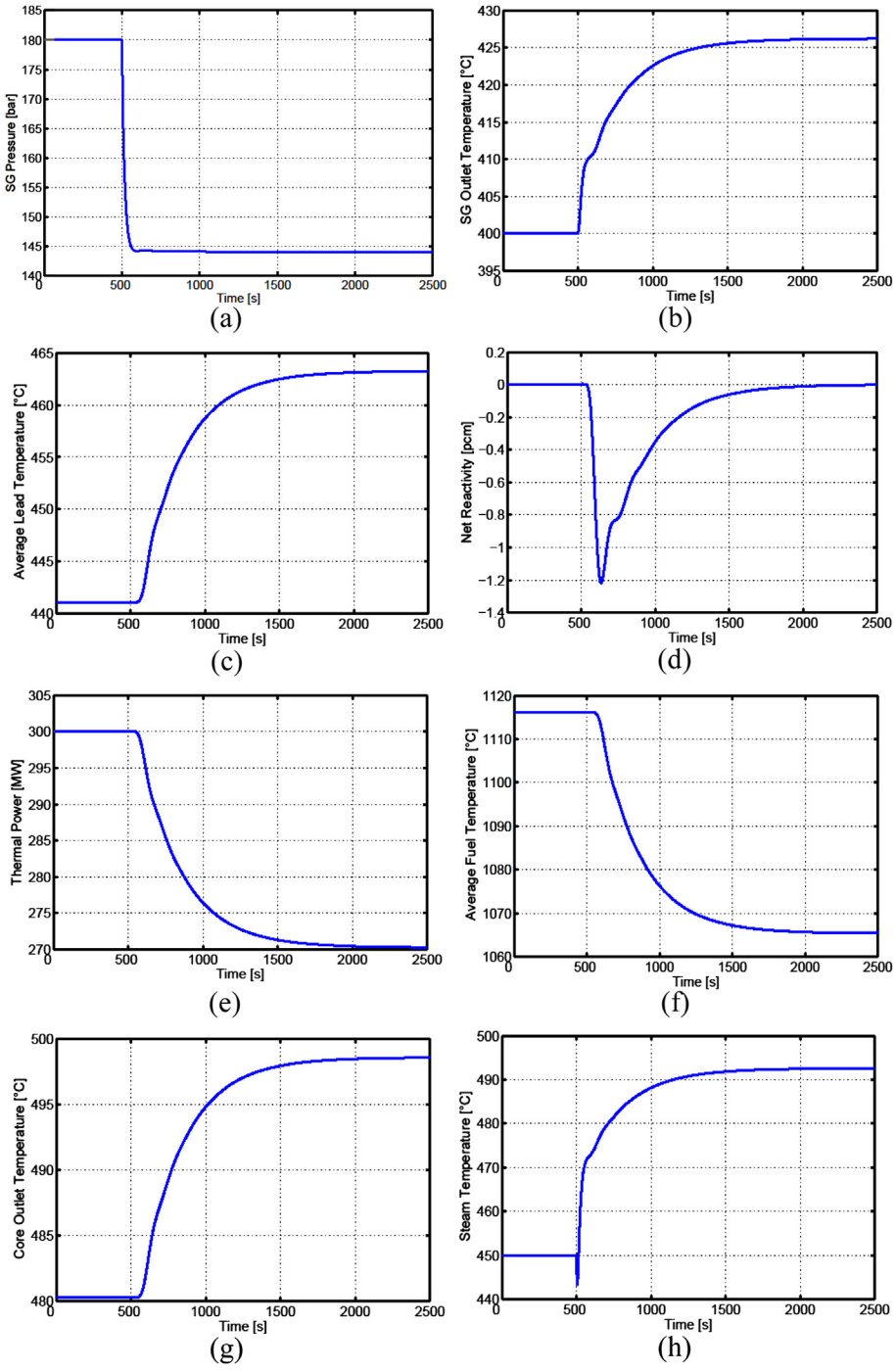

Fig. 12. Controlled variables evolution after a feedwater mass flow rate reduction: (a) SG pressure variation; (b) lead SG outlet temperature variation; (c) average lead temperature variation; (d) net reactivity variation; (e) core thermal power variation; (f) average fuel temperature variation; (g) core outlet temperature variation; (h) steam temperature variation.

decreases and a lower power transfer occurs, inducing a lead temperature enhancement at the SG outlet (Fig. 13b). The ensuing negative reactivity insertion (Fig. 13c) determines a core power reduction (Fig. 13d). As to the coolant core outlet temperature (Fig. 13e), an increase is observed even though slighter than the one at the core inlet.

It is worthwhile discussing the behaviour of the steam temperature (Fig. 13f). In the first part of the transient, its evolution is characterized by the typical dynamics of a stand-alone SG. The initial sudden rise is due to the fact that the turbine admission variation causes a mass flow rate reduction and, at constant thermal power exchanged, the steam gets hotter and hotter. Nevertheless, the overall tube is immediately affected by the pressure change and by the consequent saturation temperature increase, and therefore the overheated region within the tube gets shorter and the steam temperature decreases. After 70 s, the SG starts perceiving the effects ensuing from the core evolution and then, according to the core outlet lead temperature, the steam temperature increases until the system settles at a higher new steady-state value. The main outcome of this simulation is that, in virtue of the

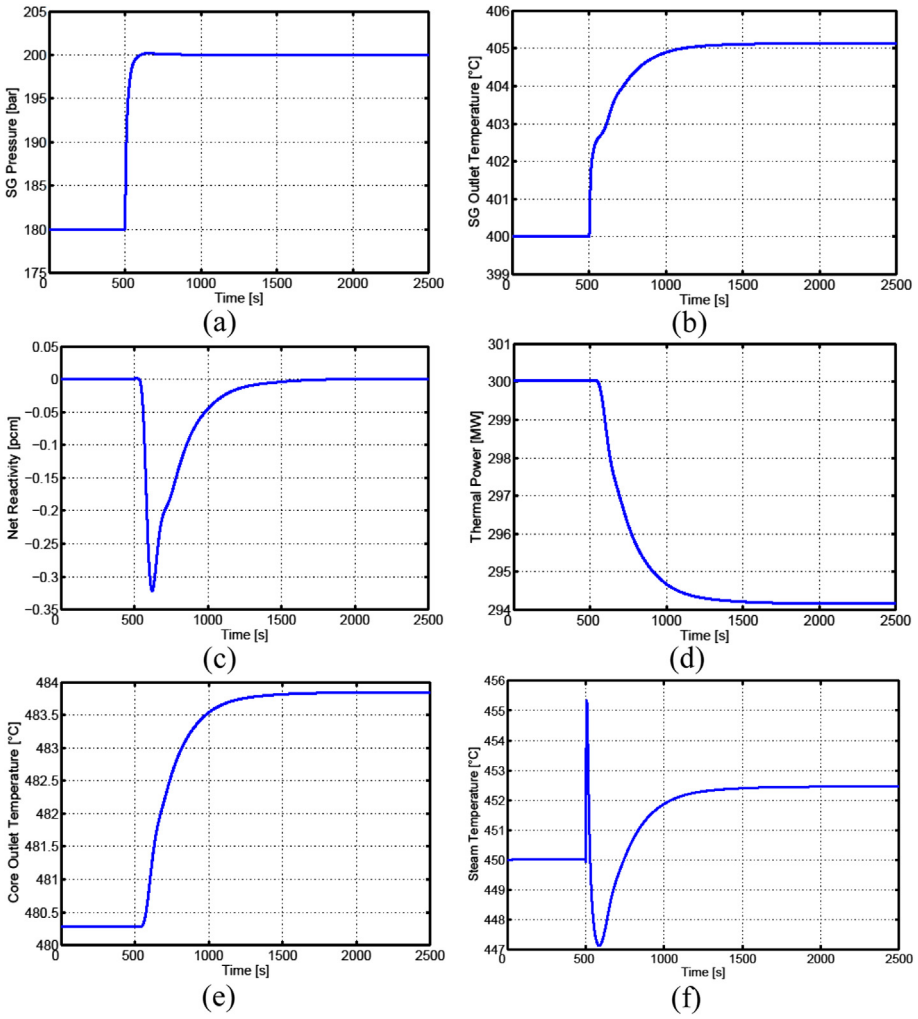

Fig. 13. Controlled variables evolution after a variation of the turbine admission valve coefficient: (a) SG pressure variation; (b) lead SG outlet temperature variation; (c) net reactivity variation; (d) core thermal power variation; (e) core outlet temperature; (f) steam temperature variation.

values assumed by the reactivity feedback coefficients, the ALFRED reactor response following the turbine admission valve variation can be considered similar to that of PWRs ("reactor follows turbine"), though the characteristic time constants are definitely longer. It is worthwhile to remind that, even this similarity with the classic and well-known PWR concept, the control scheme developed for the PWRs cannot be applied "as it is" to the LFRs due to the different constraints to be fulfilled (e.g., the lead temperature in the cold pool).

4.3. Unprotected Transient of OverPower (UTOP)

An extraction of control rods corresponding to a 20 pcm step reactivity variation (Fig. 14a) has been simulated. This is an interesting operational transient to be evaluated since it involves the dynamics associated to the handling of the control rods, and how this kind of perturbation has effect on the rest of the plant. This core-driven simulation determines an immediate feedback to the SGs due to the coolant core outlet temperature enhancement. Thanks to the presence of the pool, the action of the SGs on the core, consisting in an increase of the coolant core inlet temperature, is delayed and softened.

For the first part of transient, the behaviour of the system is the same as if a stand-alone core simulation were performed. Indeed, after the step-wise insertion of reactivity given by control rods the power suddenly increases exhibiting the typical prompt jump behaviour and, after a small decrease, starts reaching the steady-state (Fig. 14b). The reactivity insertion in the core affects the SG as a temperature enhancement of the lead coming from the core (Fig. 14c). As a direct consequence of the improved heat exchange conditions due to the hotter primary fluid, the steam temperature increases (Fig. 14d). The abrupt change of the steam density determines a perturbation in the SG pressure (Fig. 14e), which ends when the primary circuit reaches a new equilibrium condition. The higher thermal power level promotes an enhancement of the lead SG outlet temperature (Fig. 14f). As far as the core behaviour is concerned, the MOX-based fuel elements, because of the low thermal conductivity, cause a stepwise increase of fuel temperature and, consequently, of the coolant average temperatures (Fig. 14g–h), after the reactivity insertion. This response produces an immediate feedback on the system due to the Doppler effect and to lead density contribution, which cause an abrupt inversion of the reactivity evolution that quickly gets back to zero.

5. Conclusions

In this paper, the development and the performance of a plant dynamics simulator dedicated to the control design for the ALFRED reactor has been presented. The features of the object-oriented modelling language Modelica have been exploited in order to

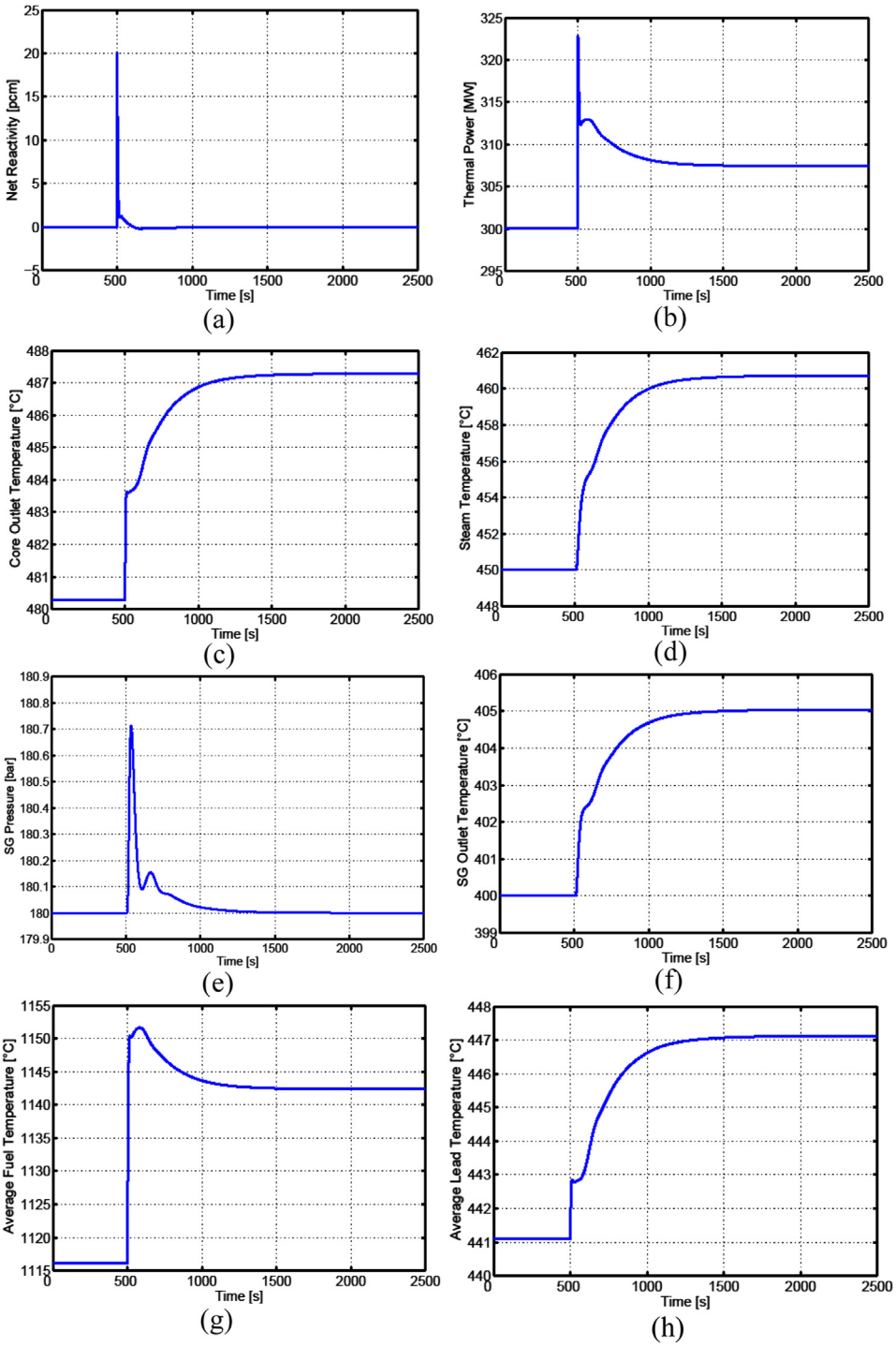

Fig. 14. Controlled variables evolution after a step reactivity variation: (a) net reactivity variation; (b) core thermal power variation; (c) core outlet temperature variation; (d) steam temperature variation; (e) SG pressure variation; (f) lead SG outlet temperature variation; (g) average fuel temperature variation; (h) average lead temperature variation.

obtain a very flexible, straightforward, and fast-running simulator aimed at performing dynamics analyses and testing in prospect the control strategies proposed for ALFRED. The simulator has been built assembling different components from the available libraries, even if some of them have been specifically set up to describe the ALFRED reactor configuration. Particular attention has been paid to the assessment of the reactivity feedback and to the bypass way with the purpose to use the simulator also for reproducing the system behaviour during other operational modes, like the start-up or the shutdown. The transport delays and the thermal inertia typical of LFR systems have been taken into account trough the adoption of dedicated components. In addition, the innovative SG bayonet tube and the secondary system up to the turbine have been modelled.

After having described the main system components and modelling assumptions, the reactor response to typical transient initiators has been investigated. As a major outcome of the dynamics analyses, the coolant cold pool and the time delays have

turned out to play an essential role in determining the system characteristic time constant due to its fundamental delaying and smoothing action on the lead core inlet temperature. Results confirm the strong coupling between core and SG, and besides show the characteristic time constants of the various component responses. The simulator has shown to provide accurate information on both transient behaviour and new equilibrium values following any perturbation concerning the main control variables.

The results of the free dynamics simulations by means of the developed simulator are thought to be useful to evaluate and develop potential control strategies. In this prospect, thanks to the possibility of linearizing the constitutive equations of the model, it would be possible to obtain the corresponding transfer functions necessary for the tuning of the controllers (i.e., a classic proportional-integral-derivative), and to characterize the linear stability features of the system. Secondly, this reliable tool can be used to prove the validity of the proposed model-based control strategies through the simulation of controlled operational transients, both for ALFRED and other innovative small-size LFR systems currently under development.

Acknowledgements

The authors acknowledge the European Commission for funding the LEADER Project in the 7th Framework Programme. Acknowledgement is also due to all the colleagues of the participant organizations for their contributions in many different topics, in particular to Dr. Alessandro Alemberti and Dr. Luigi Mansani (Ansaldo Nucleare, Italy) for their valuable support and fruitful criticism. Finally, the authors want to thank Dr. Pierre Sciora (CEA, France) for his suggestions about the ALFRED reactivity coefficients.

Nomenclature

Latin symbols

A	single channel coolant flow area [m^2]
A_{CR}	coefficient for the calibration of CRs [pcm]
A_{SR}	coefficient for the calibration of SRs [pcm]
A_v	flow area [m^2]
B_{CR}	coefficient for the calibration of CRs [m^{-1}]
Bo	boiling number [−]
c	average specific heat capacity [J kg^{-1} K^{-1}]
C_{CR}	coefficient for the calibration of CRs [−]
c_i	density of the ith precursor group [cm^{-3}]
C_f	Fanning friction coefficient [−]
Co	convection number [−]
d	density [kg m^{-3}]
D_{CR}	coefficient for calibration of CRs [pcm]
F_{Fl}	fluid−surface parameter
Fr_{LO}	Froude number with all flow as liquid
g	gravitational acceleration [m s^{-2}]
h	specific enthalpy [J kg^{-1}]
h_{CR}	height of control rods [m]
h_{LO}	single-phase heat transfer coefficient with all flow as liquid [W m^{-2} K^{-1}]
h_{SR}	height of safety rods [m]
h_{TP}	two phase heat transfer coefficient [W m^{-2} K^{-1}]
i_{LG}	latent heat of vaporization [J kg^{-1}]
k	thermal conductivity [W m^{-1} K^{-1}]
K_D	Doppler constant [pcm]
k_v	turbine admission valve coefficient [m s]
L_{SR}	total length of SRs [m]
n	neutron density [cm^{-3}]
N	number of axial nodes [−]
Nu	Nusselt number [−]
p	pressure [Pa]
Pe	Peclet number [−]
P	thermal power [W]
q	neutron source [cm^{-3} s^{-1}]
q''	heat flux [W m^{-2}]
q'''	thermal power density [W m^{-3}]
r	radial coordinate [m]
R	radius [m]
t	time [s]
T	average temperature [K]
u	fluid velocity [m s^{-1}]
w	mass flow rate [kg s^{-1}]
x	axial coordinate [m]
x_c	critical ratio [−]
x_v	vapour quality [−]
x_{SR}	height of SRs at full power [m]
z	elevation [m]

Greek symbols

α_{CR}	radial cladding expansion reactivity coefficient [pcm K^{-1}]
α_{CZ}	axial cladding expansion reactivity coefficient [pcm K^{-1}]
α_{FZ}	axial fuel expansion reactivity coefficient [pcm K^{-1}]
α_{Dia}	diagrid expansion reactivity coefficient [pcm K^{-1}]
α_L	coolant density reactivity coefficient [pcm K^{-1}]
α_{Pad}	pad effect reactivity coefficient [pcm K^{-1}]
α_{WR}	radial wrapper expansion reactivity coefficient [pcm K^{-1}]
α_{WZ}	axial wrapper expansion reactivity coefficient [pcm K^{-1}]
β	DNP total fraction [pcm]
β_i	DNP fraction of the ith precursor group [pcm]
Λ	neutron generation time [s]
λ_c	coefficient of discharge [−]
λ_i	decay constant of the ith precursor [s^{-1}]
ρ	reactivity [pcm]
ρ_0	reactivity margin stored in the core [pcm]
ϕ	heat flux entering the tube (lateral surface) [W m^{-2}]
ω	tube perimeter [m]

Superscripts

D	Doppler
eff	effective
1,2,3	fuel internal and external regions

Subscripts

0	steady-state
c	cladding
CBD	convective boiling dominant
down	downstream
f	fuel
g	gap
i	inner
in	inlet
l	lead coolant
L	liquid
NBD	nucleate boiling dominant
o	outer
out	outlet
up	upstream
V	vapour

References

Alemberti, A., Carlsson, J., Malambu, E., Orden, A., Cinotti, L., Struwe, D., Agostini, P., Monti, S., 2010. From ELSY to LEADER – European LFR activities. In:

Transactions of the American Nuclear Society, European Nuclear Conference 2010, Barcelona, Spain, May 30-June 2, 2010.
Alemberti, A., Frogheri, M., Mansani, L., 2013. The Lead fast reactor demonstrator (ALFRED) and ELFR design. In: Proceedings of the International Conference on Fast Reactors and Related Fuel Cycles: Safe Technologies and Sustainable Scenarios (FR 13), Paris, France, March 4-7, 2013.
Brenan, K.E., Campbell, S.L., Petzold, L.R., 1989. Numerical Solution of Initial-value Problems in Differential Algebraic Equations. North-Holland.
Cammi, A., Casella, F., Ricotti, M.E., Schiavo, F., 2005. Object-oriented modelling, simulation and control of IRIS nuclear power plant with Modelica. In: Proceedings of the 4th International Modelica Conference, Hamburg, Germany, March 7-8, 2005.
Cammi, A., Luzzi, L., 2008. Innovative techniques for the simulation and control of nuclear power plants. In: Durelle, V.B. (Ed.), Nuclear Energy Research Progress. Nova Science Publishers, Inc., Hauppauge, NY.
Casella, F., Leva, A., 2006. Modeling of thermo-hydraulic power generation processes using Modelica. Math. Comp. Model. Dyn. Syst. 12 (1), 19–33.
Cheng, X., Tak, N.-i., 2006. Investigation on turbulent heat transfer to lead-bismuth eutectic flows in circular tubes for nuclear applications. Nucl. Eng. Des. 236, 385–393.
Damiani, L., Montecucco, M., Pini Prato, A., 2013. Conceptual design of a bayonet-tube steam generator for the ALFRED lead-cooled reactor. Nucl. Eng. Des. 265, 154–163.
Dolezal, R., Varcop, L., 1970. Process dynamics: automatic control of steam generation plant. Elsevier Science.
Elmqvist, H., Cellier, F.E., Otter, M., 1993. Object-oriented modeling of hybrid systems. In: Proceedings of the European Simulation Symposium (ESS'93), Delft, Netherlands, October 25-28, 1993.
Fritzson, P., 2004. Principles of Object-oriented Modeling and Simulation with Modelica 2.1. Wiley-IEEE Press.
Fritzson, P., 2011. A cyber-physical modeling language and the OpenModelica environment. In: 7th International Wireless Communications and Mobile Computing Conference (IWCMC), Istanbul, Turkey, July 4-8, 2011.
GIF, 2002. A Technology Roadmap for Generation IV Nuclear Energy Systems. Technical Report GIF-002–00.
Grasso, G., Petrovich, C., Mikityuk, K., Mattioli, D., Manni, F., Gugiu, D., 2013. Demonstrating the effectiveness of the European LFR concept: the ALFRED core design. In: Proceedings of the International Conference on Fast Reactors and Related Fuel Cycles: Safe Technologies and Sustainable Scenarios (FR 13), Paris, France, March 4-7, 2013.
Kozlowski, T., Downar, T.J., 2007. PWR MOX/UO_2 Core Transient Benchmark. Working Party on Scientific Issues of Reactor Systems. Nuclear Science NEA/NSC/DOC(2006)20, ISBN 92-64-02330-5.
MATLAB® and SIMULINK® software, 2005. The MathWorks, Inc.
Modelica, 2011. http://www.modelica.org.
OECD-NEA, 2007. Handbook on Lead-Bismuth Eutectic Alloy and Lead Properties, Materials Compatibility. Thermal Hydraulics and Technologies, No. 6195.
Sciora, P., 2013. Private Communication.
Souyri, A., Bouskela, D., Pentori, B., Kerkar, N., 2006. Pressurized water reactor modelling with Modelica. In: Proceedings of the 5th International Modelica Conference, Vienna, Austria, September 4-5, 2006.
Todreas, N., Kazimi, M.S., 2012. Nuclear Systems – Thermal Hydraulic Fundamentals, second ed., vol. 1. CRC Press.
Tucek, K., Carlsson, J., Wider, H., 2006. Comparison of sodium and lead-cooled fast reactors regarding reactor physics aspects, severe safety and economical issues. Nucl. Eng. Des. 236, 1589–1598.
Waltar, A.E., Todd, D.R., Tsvetkov, P.V., 2012. Fast Spectrum Reactors. Springer, New York.